Enhanced Circular Polarization in a Hexagonal Antenna Array With Sequential Rotation

Gorka Casasus-Goyeneche*, Miguel Ferrando-Rocher*, Javier Vera-Sánchez*, and Miguel Ferrando-Bataller*
*Antennas and Propagation Lab, iTEAM Research Institute, Universitat Politècnica de València, Valencia, Spain,
jcasgoy@upv.es

***Abstract*—This paper investigates the use of sequential rotation to synthesize circular polarization at the array level, enabling robust CP performance in array layouts that are not inherently circularly symmetric. Three antenna-array configurations are examined: square, triangular, and hexagonal. For each topology, a detailed electromagnetic analysis reveals that strong coupling between the antenna elements and the ground plane plays a decisive role in the overall performance. Under simultaneous excitation of the six elements in the selected hexagonal array, the design achieves a maximum directivity of 14.10 dBi, a radiation efficiency of 85%, and an axial ratio below 1 dB across the main-beam region, confirming the generation of a high-purity circularly polarized field. The results validate the feasibility of employing sequential rotation in hexagonal layouts and highlight their potential for compact, wideband, and highly directive circularly polarized antennas.**

I. Introduction

In recent years, circular polarization (CP) plays a critical role in many modern communication systems, particularly in satellite and space-based applications. When electromagnetic waves propagate through the ionosphere, the Faraday effect can rotate the polarization plane of linearly polarized signals, potentially degrading link reliability or causing severe polarization mismatch losses [1]. Circular polarization overcomes this limitation by providing immunity to such rotations, ensuring stable reception regardless of satellite attitude, link geometry, or ionospheric conditions. Furthermore, CP offers practical benefits on the ground segment, as a circularly polarized wave can be received with minimal loss using either circularly or linearly polarized antennas. Despite these advantages, achieving high-purity circular polarization often requires introducing geometric perturbations or complex feeding schemes, which increases the design and manufacturing complexity of the antenna element.

In practice, achieving high-purity circular polarization typically requires introducing additional geometric perturbations, feed networks, or complex excitation schemes at the antenna-element level as is presented in [2]–[4]. These strategies often increase the design complexity, narrow the operational bandwidth, or place tight manufacturing constraints on the radiating structure.

In addition, as demonstrated in [5], circular polarization can also be synthesized at the array level even when the individual radiating elements are linearly polarized. This is achieved through sequential rotation, a technique in which each element within a subarray is progressively rotated in angle and fed with a corresponding progressive phase shift. When properly implemented, the collective radiation of the rotated elements produces a circularly polarized far-field response with enhanced axial ratio, broader operational bandwidth, and reduced sensitivity to element-level imperfections [6]–[8].

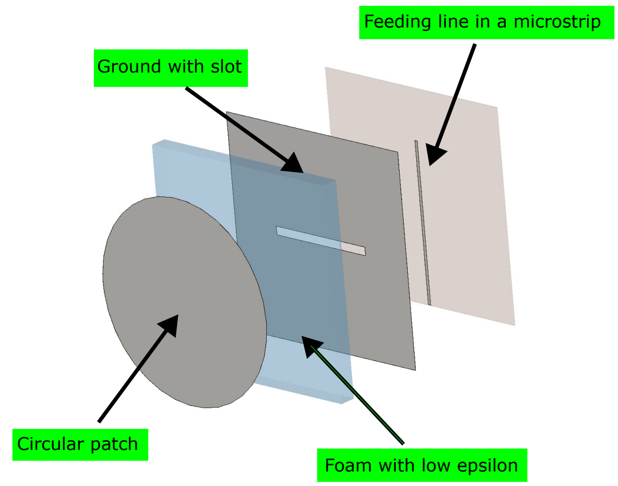

Fig. 1. Unit-cell geometry consisting of a circular patch antenna excited by a slot coupled to a microstrip feed.

Most implementations of sequential rotation reported in the literature rely on conventional 2×2 rectangular subarray configurations, where the rotation angles and phase increments follow well-established patterns of 0°, 90°, 180° and 270° like in [9]. Nevertheless, the underlying principle is more general and can be extended to other array layouts. Arrays arranged in triangular or hexagonal lattices, or other non-rectangular geometries can also benefit from sequential rotation, although the corresponding rotation rules and phase relationships are not as straightforward and require dedicated analysis [10].

This paper investigates the application of sequential rotation to different array layouts. For each geometry, the achievable circular polarization is analyzed as a function of the dominant current orientation, distinguishing between tangential and radial directions depending on the slot position. A simple, low-profile, and compact design is then identified, achieving good directivity while preserving excellent axial-ratio performance and polarization purity.

II. Unit Cell

To simplify the complexity of the designs presented in this work, a linearly polarized unit cell is adopted, since circular polarization will be synthesized at the array level. Each radiating element consists of a circular microstrip patch

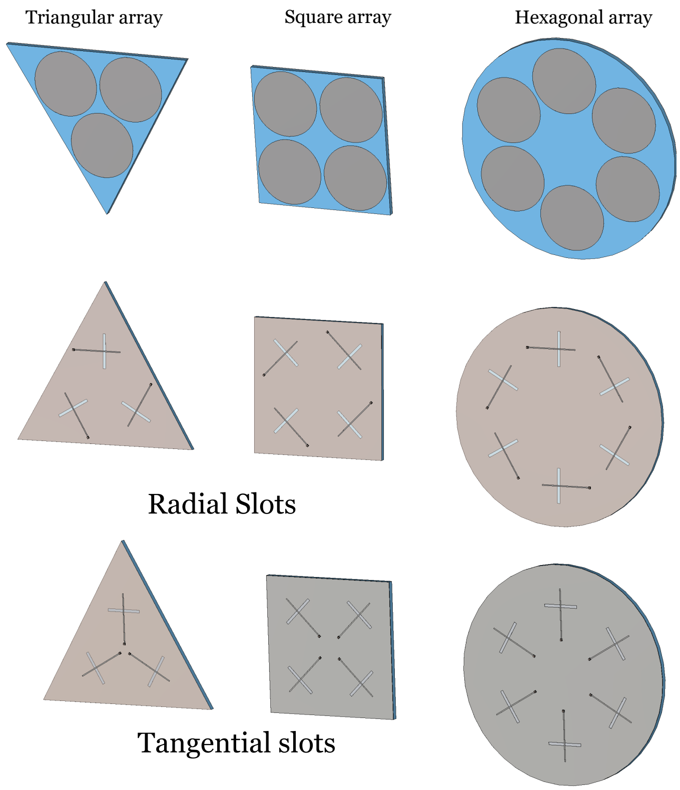

Fig. 2. Geometrical layout of the analyzed designs using microstrip feeding for tangential and radial slots.

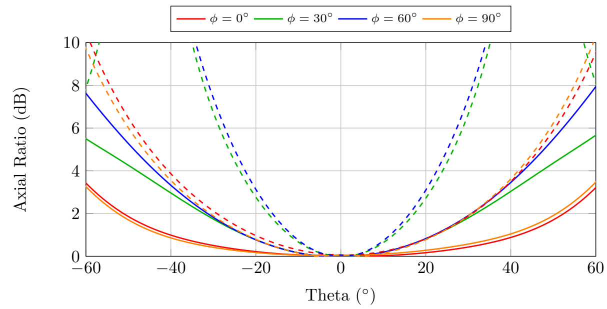

Fig. 3. Axial ratio of the square array with tangential slots (solid) and radial slots (dashed).

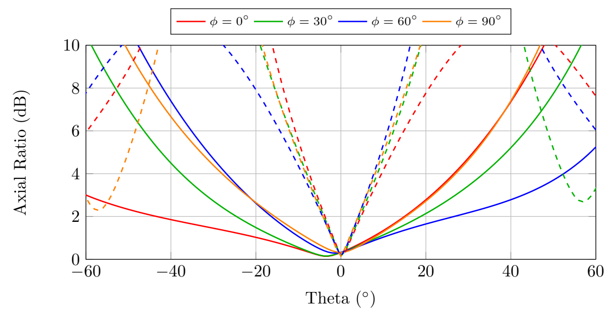

Fig. 4. Axial ratio of the triangular array with tangential slots (solid) and radial slots (dashed).

with a radius of 60 mm, placed over a Rohacell substrate with a relative permittivity of $\varepsilon_r = 1.006$. The patch is excited through a rectangular slot fed by a microstrip line implemented on a Rogers RO4003C substrate. This configuration provides a realistic, manufacturable solution that serves as the baseline for evaluating the effect of sequential rotation. The corresponding geometry is shown in Fig. 1.

III. Sequential Rotation in Different Structures

This section evaluates the electromagnetic performance of three antenna array configurations: square, triangular, and hexagonal (Fig. 2), where sequential rotation is applied. For each array, two slot orientations, tangential and radial with respect to the array center, were analyzed, resulting in distinct circular-polarization behavior depending on the geometry.

The square 2×2 array, taken as the canonical reference, achieves sequential rotation by rotating each element by $90°$ while maintaining coincident excitation phases. This well-known scheme produces high-quality circular polarization, with an axial ratio close to 0 dB in the main lobe. As shown in Fig. 3, tangential slots provide a slightly purer CP and extend the angular region in which the axial ratio remains below 3 dB, though these improvements occur outside the useful scanning range. Consequently, both slot orientations perform adequately within the effective radiation region of the array.

In the triangular array, each antenna must be fed with a $120°$ phase shift to implement sequential rotation. In this case, the influence of slot orientation becomes more pronounced. Radial slots still enable circular polarization at boresight; however, as shown in Fig. 4, the axial ratio degrades rapidly away from the main beam, limiting the CP coverage to approximately $\pm10°$, which is narrower than the main-lobe beamwidth. Tangential slots mitigate this degradation significantly, maintaining a lower axial ratio over a wider angular span of roughly $\pm20°$. Therefore, the tangential orientation proves more suitable for this non-canonical geometry.

Conversely, in the hexagonal array, the trend is reversed. Under the required $60°$ phase progression, the increased geometric symmetry of the hexagon yields a more balanced field distribution, and in this case the radial slot orientation provides the best circular-polarization performance (Fig. 5). While tangential slots still produce acceptable results, radial slots maintain a considerably lower axial ratio across the entire main lobe, offering a more uniform and robust CP behavior. This improvement is attributed to the better alignment between the radial surface currents and the intended rotating field components inherent to the hexagonal layout, as illustrated in Fig. 6, where the average electric-field distribution of both slot orientations is compared.

IV. Design of a Hexagonal Array

Given that the hexagonal array exhibited the most promising results, it was selected for a more detailed analysis with the

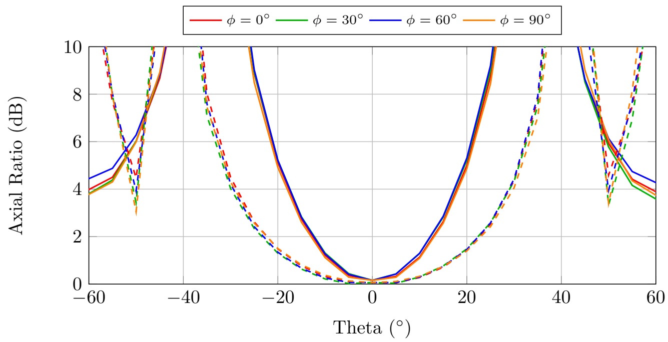

Fig. 5. Axial ratio of the hexagonal array with tangential slots (solid) and radial slots (dashed).

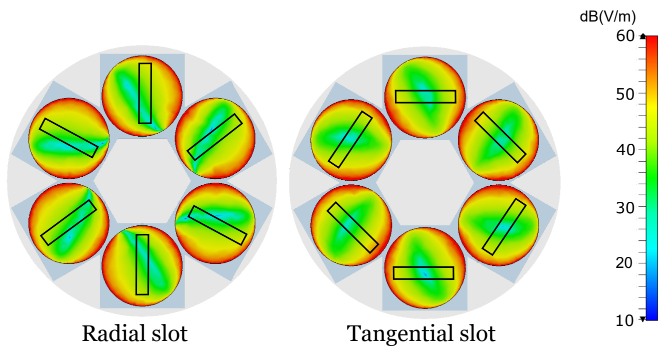

Fig. 6. Average electric-field distribution of the hexagonal array with radial slots (left) and tangential slots (right).

objective of developing a functional design combining high efficiency, good directivity, low axial ratio, and a structurally simple layout. A closer examination of the radiated fields revealed a strong coupling between the antenna elements and the ground plane. This interaction causes the ground plane to become the predominant radiating surface, which helps explain the enhanced directivity. The corresponding time-varying electric-field distribution on the ground plane is shown in Fig. 7.

All six elements are properly matched at the operating frequency $f_0 = 1150$ MHz achieving a 50 MHz bandwidth, as illustrated in Fig. 8, where the active S-parameters are shown under the condition of simultaneous excitation of the six antennas. Under this operating regime, the array attains a maximum directivity of 14.10 dBi and an efficiency of 85 % (-0.7067 dB).

The radiation characteristics further confirm the robustness of the design. As depicted in Fig. 9, the main beam exhibits radial symmetry with a -3 dB beamwidth covering the angular range from $-18°$ to $18°$. Additionally, Fig. 5 from the previous chapter shows that the axial ratio remains below 1 dB throughout this interval, demonstrating that the antenna maintains an almost pure circular polarization across the region of interest.

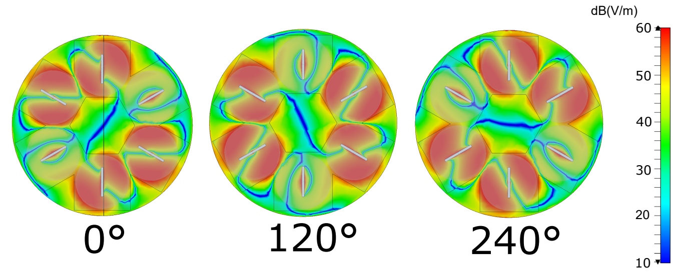

Fig. 7. Instantaneous electric-field distribution on the ground plane for excitation phases of 0°, 120°, and 240°.

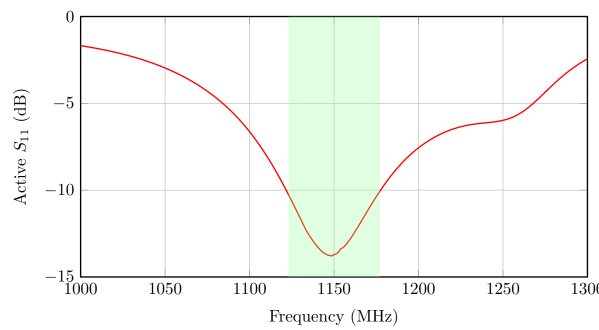

Fig. 8. Active S-parameters of the hexagonal array with sequential-rotation feeding.

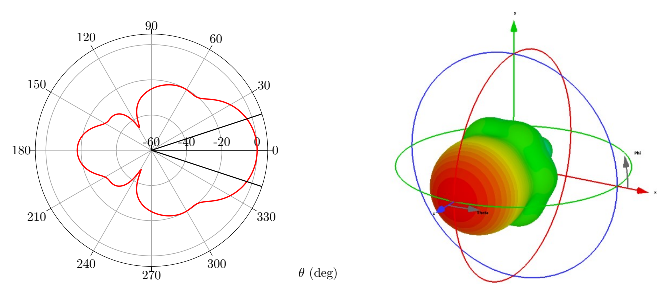

(a) (b)

Fig. 9. Radiation pattern of the hexagonal antenna: $\phi = 0$ cut (a) and 3D (b).

V. Conclusion

This work has demonstrated that sequential rotation can be effectively extended beyond conventional square configurations to triangular distribution arrays, enabling robust circular polarization and improved radiation performance in geometries that traditionally lack inherent symmetry. Among the different topologies evaluated, the hexagonal array exhibited the most balanced and promising behavior, combining low axial ratio, well-controlled matching, and enhanced directivity within a compact and structurally simple footprint.

A detailed electromagnetic analysis revealed that the strong coupling between the antenna elements and the ground plane plays a decisive role in the performance of the proposed design. This interaction causes the ground plane to become the dominant radiating surface, thereby contributing to the observed improvement in directivity. This effect enables a simplified implementation that outperforms similar antenna solutions such as the one reported in [11]. Under simultaneous excitation of the six elements, the array achieves a maximum directivity of 14.10 dBi, an efficiency of 85 %, and an axial ratio below 1 dB across the main-beam region, confirming the generation of an almost pure circularly polarized field.

Overall, the results validate the feasibility of employing sequential rotation in hexagonal layouts and highlight their potential as an attractive alternative for applications requiring compact, wideband, and highly directive circularly polarized antennas. Future work will address the optimization of the feeding network, integration into planar platforms, and the extension of the methodology to larger arrays.

ACKNOWLEDGEMENT

This research is part of the SATERA project, supported by the SESAR 3 Joint Undertaking (JU) under grant agreement No. 101164313, with additional funding from Spain's Ministerio de Ciencia e Innovación under research projects PID2022-136869NB-C33, PID2022-141055NB-C21 and INDRA Espacio S.L.U. under the LINCE project of the Spanish Space Technology Program.

REFERENCES

[1] N. D. Tripathi and J. H. Reed, *Challenges of an NTN*, 2026, pp. 87–104.

[2] D. K. Naik, D. Charan Panda, R. Swain, A. Muduli, and S. Nanda, "Pac-man-shaped patch-driven broadband circularly polarized metasurface antenna with cma-based quadruple-mode excitation," *IEEE Access*, vol. 13, pp. 13 644–13 654, 2025.

[3] Y. Xu, H. Hu, B. Chen, M. Chen, J. Tian, and S. Lei, "Broadband high-gain circularly polarized antenna for conformal applications," *IEEE Antennas and Wireless Propagation Letters*, vol. 22, no. 8, pp. 2032–2036, 2023.

[4] H. Yang, Y. Fan, and X. Liu, "A compact dual-band stacked patch antenna with dual circular polarizations for beidou navigation satellite systems," *IEEE Antennas and Wireless Propagation Letters*, vol. 18, no. 7, pp. 1472–1476, 2019.

[5] J. Huang, "A technique for an array to generate circular polarization with linearly polarized elements," *IEEE Transactions on Antennas and Propagation*, vol. 34, no. 9, pp. 1113–1124, 1986.

[6] H. W. Lai, D. Xue, H. Wong, K. K. So, and X. Y. Zhang, "Broadband circularly polarized patch antenna arrays with multiple-layers structure," *IEEE Antennas and Wireless Propagation Letters*, vol. 16, pp. 525–528, 2017.

[7] D.-F. Guan, B. Fang, Y.-S. Zhang, W. Shao, and J.-H. Shen, "Broadband siw cavity-backed circularly polarized antenna element and array," in *2015 IEEE International Wireless Symposium (IWS 2015)*, 2015, pp. 1–4.

[8] S. X. Ta and I. Park, "Compact wideband circularly polarized patch antenna array using metasurface," *IEEE Antennas and Wireless Propagation Letters*, vol. 16, pp. 1932–1936, 2017.

[9] W. Yang, J. Zhou, Z. Yu, and L. Li, "Bandwidth- and gain-enhanced circularly polarized antenna array using sequential phase feed," *IEEE Antennas and Wireless Propagation Letters*, vol. 13, pp. 1215–1218, 2014.

[10] H. K. Kan and R. Waterhouse, "A small CP-printed antenna using 120/spl deg/ sequential rotation," *IEEE Transactions on Antennas and Propagation*, vol. 50, no. 3, pp. 398–399, 2002.

[11] H. Liao and A. Shamim, "A low-profile and high-aperture-efficiency hexagonal circularly polarized microstrip antenna array," *IEEE Antennas and Wireless Propagation Letters*, vol. 21, no. 3, pp. 615–619, 2022.